

PAPER • OPEN ACCESS

Caloric effects in liquid crystal-based soft materials

To cite this article: Devid Črešnar *et al* 2023 *J. Phys. Energy* 5 045004

View the [article online](#) for updates and enhancements.

You may also like

- [\(Invited\) Stimuli Responsive Liquid Crystal Elastomers/Gels](#)
Kenji Urayama
- [The Low-redshift Lyman Continuum Survey. I. New, Diverse Local Lyman Continuum Emitters](#)
Sophia R. Flury, Anne E. Jaskot, Harry C. Ferguson et al.
- [Theory of giant-caloric effects in multiferroic materials](#)
Melvin M Vopson



PAPER

Caloric effects in liquid crystal-based soft materials

OPEN ACCESS

RECEIVED
8 June 2023REVISED
5 August 2023ACCEPTED FOR PUBLICATION
16 August 2023PUBLISHED
25 August 2023

Original content from this work may be used under the terms of the [Creative Commons Attribution 4.0 licence](https://creativecommons.org/licenses/by/4.0/).

Any further distribution of this work must maintain attribution to the author(s) and the title of the work, journal citation and DOI.



Dejvid Črešnar^{1,2} , Nikita Derets^{1,2} , Maja Trček¹ , Gregor Skačej³ , Andraž Rešetič¹ , Marta Lavrič¹ , Valentina Domenici⁴ , Boštjan Zalar¹ , Samo Kralj^{1,2,5} , Zdravko Kutnjak^{1,2} and Brigita Rožič^{1,2,*}

¹ Condensed Matter Physics Department, Jožef Stefan Institute, Ljubljana, Slovenia

² Jožef Stefan International Postgraduate School, Ljubljana, Slovenia

³ Faculty of Mathematics and Physics, University of Ljubljana, Ljubljana, Slovenia

⁴ Dipartimento Di Chimica E Chimica Industriale, Università Di Pisa, Pisa, Italy

⁵ Department of Physics, Faculty of Natural Sciences and Mathematics, University of Maribor, Maribor, Slovenia

* Author to whom any correspondence should be addressed.

E-mail: brigita.rozic@ijs.si

Keywords: electrocaloric, elastocaloric, liquid crystal, liquid crystal elastomers

Supplementary material for this article is available [online](#)

Abstract

With the increased environmental awareness, the search for environmentally friendlier heat-management techniques has been the topic of many scientific studies. The caloric materials with large caloric effects, such as the electrocaloric (EC) and elastocaloric (eC) effects, have increased interest due to their potential to realize new solid-state refrigeration devices. Recently, caloric properties of soft materials, such as liquid crystals (LCs) and LC elastomers (LCEs), are getting more in the focus of caloric materials investigations, stimulated by large caloric effects observed in these materials. Here, an overview of recent direct measurements of large caloric effects in smectic LC 14CB and main-chain LCEs is given. Specifically, high-resolution thermometric measurements revealed a large EC response in 14CB LC exceeding 8 K. Such a large effect was obtained at a relatively moderate electric field of 30 kV cm⁻¹ compared to solid EC materials. We demonstrate that such a small field can induce the isotropic to smectic A phase transition in 14CB, releasing or absorbing relatively large latent heat that enhances the EC response. Furthermore, it is demonstrated that in main-chain LCEs, the character of the nematic to isotropic transition can be tuned from the supercritical towards the first-order regime by decreasing the crosslinkers' density. Such tuning results in a sharper phase transition and latent heat that enhance the eC response, exceeding 2 K and with the eC responsivity of 24 K MPa⁻¹, about three orders of magnitude larger than the average eC responsivity found in the best shape memory alloys. Significant caloric effects in soft LC-based materials, observed at much smaller fields than in solid caloric materials, demonstrate their ability to play an important role as new cooling elements, thermal diodes, and caloric-active regeneration material in new heat-management devices.

1. Introduction

Caloric effects, such as magnetocaloric (MC), electrocaloric (EC) and mechanocaloric (mC) effects, are related to a reversible change in the temperature ΔT of material upon switching a field/stress on or off under quasi-adiabatic condition (figures 1(a) and (b)). With potential use in various heat-management applications, such as cooling devices and heat pumps, caloric effects recently became very attractive. New-generation devices exploiting solid-state caloric effects should have better energy efficiency and be environmentally friendlier [1–8].

The EC effect (ECE) is found in materials with the electric field conjugated to the order parameter or coupling through the anisotropy of susceptibility tensor, i.e., in ferroelectric materials or dielectrics with inducible dipoles, respectively [2–10]. A coupling of the electric field to the order parameter enables manipulation of the dielectric subsystem entropy by changing the external electric field [3].

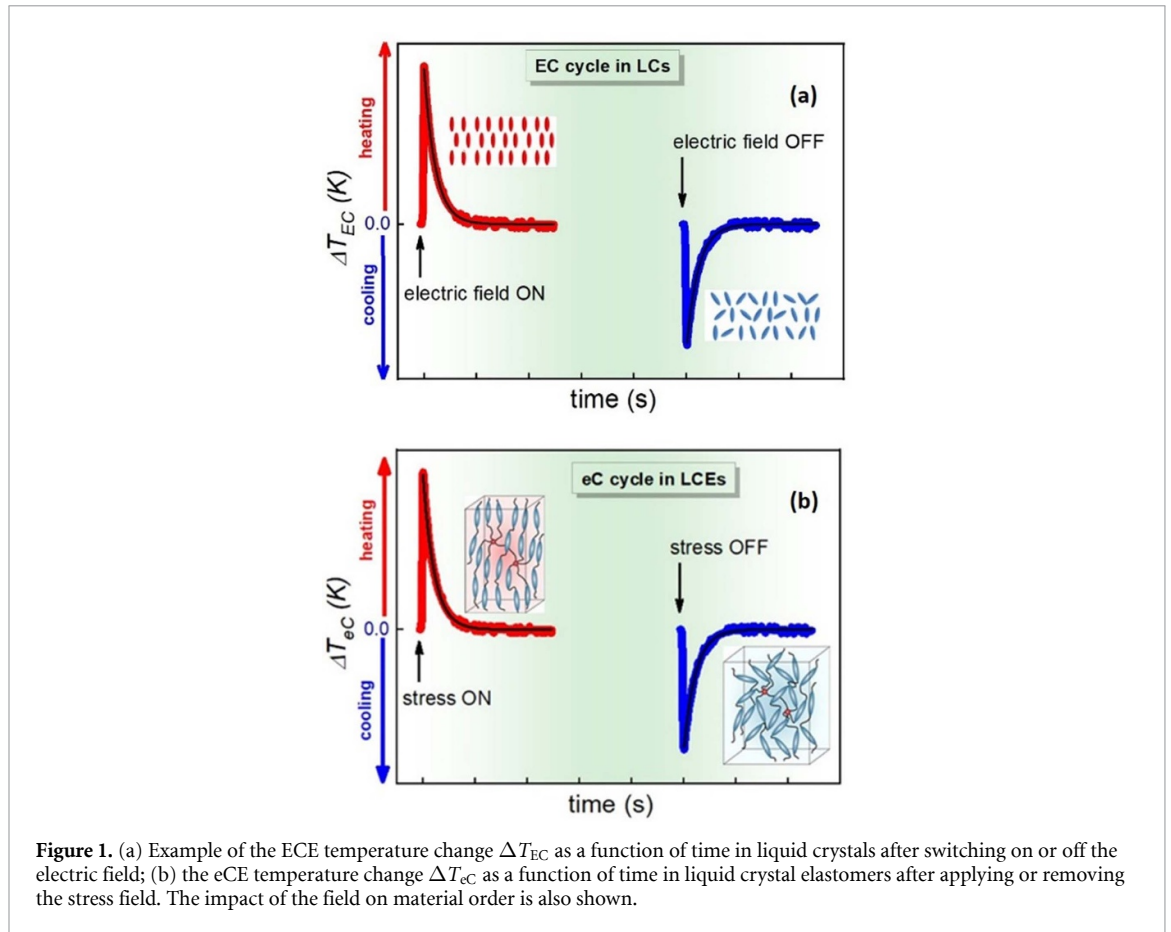


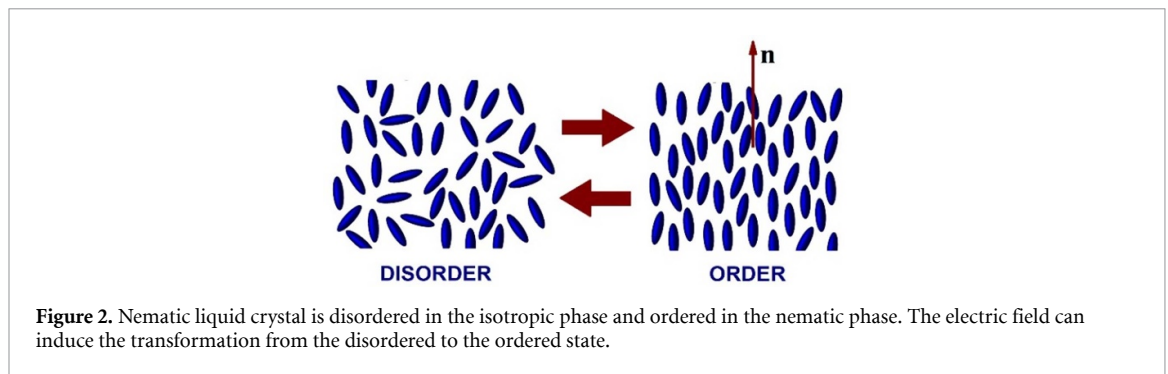
Figure 1. (a) Example of the ECE temperature change ΔT_{EC} as a function of time in liquid crystals after switching on or off the electric field; (b) the eCE temperature change ΔT_{eC} as a function of time in liquid crystal elastomers after applying or removing the stress field. The impact of the field on material order is also shown.

In quasi-adiabatic conditions, the EC heating or cooling of an EC material manifests the entropy exchange between the two entropy reservoirs, i.e., the field-ordering and thermal vibrational subsystems, in such a way that the total entropy remains preserved [9]. For example, the applied electric field induces dipolar ordering, hence the reduction of the entropy of the dipolar state in a dielectric material, and vice versa, when an electric field is removed [3–12]. Typically, such changes can be considered adiabatic as they take place in a much shorter time than the characteristic time of the heat flow from the material to the surrounding bath. Therefore, as the total entropy of a dielectric material remains preserved, the increase of the thermal subsystem entropy compensates for the drop in a dipolar subsystem entropy. Consequently, the temperature of the material is increased, and vice versa, if the field is removed (figure 1(a)), in an analogy to other caloric effects such as the elastocaloric (eC) effect in liquid crystal elastomers (LCEs) (figure 1(b)) [13].

Ferroelectric materials with polarization order parameter linearly coupled to the electric field are currently the best and most studied examples of EC systems. Observation of the giant EC effect, both in inorganic perovskite ferroelectric thin films [2–9, 11, 14, 15] and in organic, P(VDF-TrFE) based ferroelectric copolymers [1, 16, 17], initiated the revival of caloric effects studies and development of first proof of concept cooling devices from these solid state materials [8, 18, 19]. However, these devices suffer low power density due to the relatively large mass of EC-inactive regenerator fluids. Replacing the EC-inactive fluid regenerator with the EC-active dielectric fluid, such as nematic liquid crystals (LCs), could solve this problem.

In nematic LCs, the nematic uniaxial orientational order parameter S is coupled to the electric field E via dielectric anisotropy term $-\epsilon_0 \Delta \epsilon E^2 S$. Here, $\Delta \epsilon$ represents the anisotropy of the dielectric tensor. The application of the field thus enables the ordering of the molecules along the average nematic director n (figure 2), i.e., the transformation from the disordered isotropic state to the ordered nematic state (also see electric field-temperature (E - T) schematic phase diagram in figure 3). Early investigations showed that ECE of 0.5–2 K is expected in nematic LC 5CB with a nematic entropy change of 23 J kg^{-1} at 900 kV cm^{-1} electric field change [20–22].

Recently, it was demonstrated that much stronger ECE is expected in LC systems close to the isotropic–nematic–smectic A (I-N-SmA) triple point. In such systems, besides the orientational, also translational mesoscopic scale smectic ordering exists, described by the translational order parameter field η [23]. The coupling between the orientational and the translational order parameters through the free energy term $-D\eta^2 S$ enables the electric field to induce entropy changes in both energy reservoirs [23–25]. Suitable



materials are higher homologues of the *n*-alkyl cyanobiphenyl family of LCs (nCBs, $n = 5-14$) [23, 24, 26]. Homologues above the I-N-SmA triple point ($n > 10$) exhibit the direct first-order I-SmA phase transition with substantial latent heat that might provide an additional boost to the EC response [3, 23, 24, 27]. Indeed, the direct EC measurements confirmed the existence of a large ECE exceeding 6 K in 12CB [24]. However, due to the proximity of 12CB to the I-N-SmA triple point and the relatively high electric field of 80 kV cm^{-1} used, the latent heat's importance was unclear.

Another promising caloric effect was recently reported in soft materials, i.e., eC effect (eCE) in LCEs [23]. In eC systems, a stress field σ is coupled with the strain $\varepsilon = \Delta l/l$. Currently, the best material examples exhibiting very large eCE are shape memory alloys [5–8, 15, 28–30]. Specifically, in Ni50.2Ti49.8 shape memory alloy wires, the eC temperature change of 40 K was measured at the applied stress of 0.8 GPa [15, 28–30]. In addition, it was recently demonstrated that these materials could serve effectively as a coolant in heat pumps [5, 7, 30]. However, such devices require rather heavy stress actuators due to the significant stress fields required, making miniaturization of such cooling devices difficult.

Potential material candidates that can remedy this issue can be found among soft LCE materials exhibiting the giant thermomechanical response, in which orders of magnitude smaller stress fields could still produce sizable entropy changes [31, 32]. Two main types of LCEs are currently synthesized: side-chain and main-chain LCEs. In side-chain LCEs, the elastomer polymer network is crosslinked by crosslinking molecules (crosslinkers), and LC mesogens that compose most of the mass of LCEs are side-attached to polymer chains [31, 32]. In contrast, the mesogens in main-chain LCEs are components of polymer chains and are thus parts of the polymer network. A large thermomechanical effect observed in LCEs results from an internally-imprinted stress field in the polymer network memory during the second crosslinking step [31, 32]. Specifically, the polymer network is weakly crosslinked in the first step, forming an elastomer. In the second step, the LCEs are stretched by the external stress field so that mesogens form the nematic structure, and then by crosslinking, the corresponding internal stress field is imprinted [32]. As a consequence of such imprinted-stress memory, a large thermomechanical effect can be observed in LCEs, in which, by changing the temperature, strains up to 400% could be observed in main-chain LCEs [31].

As the external stress field σ is directly coupled to the nematic order parameter S in LCEs, applying the external stress field would induce nematic entropy changes and, thus, an eC response (figure 1(b)). It was shown recently that the eCE could be tuned from supercritical toward the first order type [33]; however, the critical point [31] was not reached. Therefore the eC response near the critical point in LCEs still requires detailed studies through simulations and experiments.

In this work, we will address the two caloric effects in soft materials by direct experimental methods. The first section will present direct measurements of the EC response in smectic LC 14CB. The direct measurements near the critical point and molecular Monte Carlo (MC) simulations of the eC effect in main-chain LCE will be discussed in the next section. The final section will discuss the importance and summary of the above results.

2. EC effect in smectic LC 14CB: experiment and discussion

2.1. Experimental

The high-purity smectic LC 4-*n*-tetradecyl-4'-cyanobiphenyl or 14CB that exhibits a direct isotropic to SmA phase transition on cooling was synthesized at Likchem, Warsaw, Poland (with mentioned purity higher than 99.92%). The sample was additionally purified by recrystallization to minimize the Joule heating due to the leakage current of ionic impurities.

Typically, 10 mg samples of 14CB were prepared by loading 14CB into a high-purity glass cell made of two $140 \mu\text{m}$ thick glass plates coated by indium tin oxide (ITO) electrodes and separated by a $120 \mu\text{m}$ thick

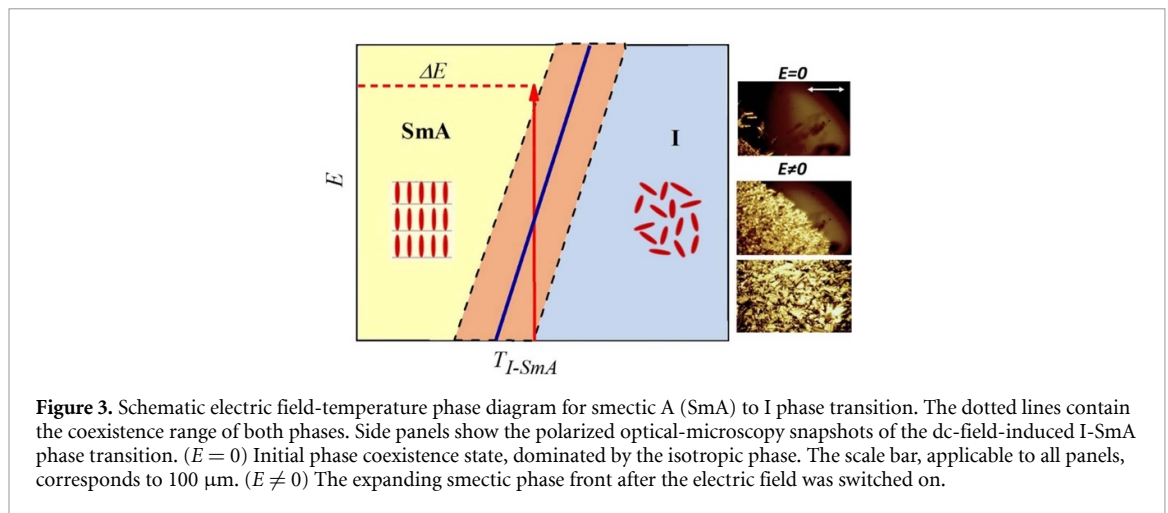


Figure 3. Schematic electric field-temperature phase diagram for smectic A (SmA) to I phase transition. The dotted lines contain the coexistence range of both phases. Side panels show the polarized optical-microscopy snapshots of the dc-field-induced I-SmA phase transition. ($E = 0$) Initial phase coexistence state, dominated by the isotropic phase. The scale bar, applicable to all panels, corresponds to 100 μm . ($E \neq 0$) The expanding smectic phase front after the electric field was switched on.

Mylar spacer (figure S1). We chose not to use a high-speed, high-resolution IR camera for ECE and eCE estimations as preliminary studies showed serious challenges in determining the sample-cell system's emissivity, transmissivity and reflectivity. As 14CB LC or LCEs undergo phase transformation induced by the field or temperature, the emissivity and transmissivity of the sample changes, rendering precise estimation of ECE practically impossible, similarly as in the case of thin P(VDF-TrFE-CFE) free-standing films recently described in [34]. Instead, the temperature variation of the whole cell system was measured in a classic thermometric way described in [2, 3] using a small-bead thermistor attached to the glass plate mounted in a sample-holder head of the high-resolution calorimeter (see figures S1 and S2).

The experimental details and the ECE measurement protocol are given in [2, 3, 23, 35, 36]. At each temperature, the 30 kV cm^{-1} electric field single square-shaped pulse was applied starting from zero. The applied field was slightly stronger than 12 kV cm^{-1} , required to induce the I-SmA phase transition near the coexistence range fully. However, a somewhat higher electric field enables ECE measurements about 0.5 K deeper in the I phase.

The duration of the electric pulse of 520 s was several times longer than the external thermal time scale of $\tau_{\text{ext}} \approx 100$ s, in which the cell reaches thermal equilibrium with the surrounding bath (see figure S3). The EC response was measured immediately after the rising edge of the pulse and after the falling edge. As described in [2, 3], the relaxation of the temperature of the whole cell system back to the bath temperature was monitored, $T(t) = T_{\text{bath}} + \Delta T \exp(-t/\tau)$, after it has reached internal equilibration within $\tau_{\text{int}} \approx 20$ s. The ECE temperature change of the 14CB was obtained by taking into consideration the heat capacities of its constituents, C_p^i , such as the sample, glass plates, glue, thermistor, attaching wires, and the geometry of the sample cell, $\Delta T_{\text{EC}} = \Delta T \sum_i C_p^i / C_p^{\text{EC}}$. Here, C_p^{EC} denotes the heat capacity of the EC active material, i.e., 14CB under the ITO electrodes. It should be noted that similar to 12CB [23], small Joule heating was observed on the order of 20% of the maximum EC temperature change, shown as an elevated plateau at longer times when the field is switched on (see figure S3). The amplitude of the Joule heating can be discerned from the saturated plateau at longer times. As Joule heating follows exponential relaxation with the same external and internal times, it can be easily subtracted from the data to reveal the actual intrinsic EC response of the sample [23].

14CB is a higher homologue of the nCB family of LCs, even further away from the I-N-SmA triple point, located between $n = 9$ and 10 [26]. In 14CB, the latent heat (L) released at the direct isotropic to smectic A transition is even higher $L = 14.7 \text{ J g}^{-1}$ compared to the latent heat $L = 12.2 \text{ J g}^{-1}$ of 12CB [23]. Therefore, the maximum EC response in 14CB is expected at the melting I-SmA phase transition. The dominant contribution of the latent heat to the ECE response is achieved only by using sufficiently small fields that do not induce sizeable continuous entropy changes. As the latent heat is released within the coexistence range of isotropic and smectic phases (contained between two dotted lines in the E - T phase diagram presented in figure 3), the electric field (ΔE) that induces the changes ending just above the coexistence range should suffice in checking the latent heat contribution.

Polarized optical microscopy shows that with the electric field switched on, the smectic phase front expands until all sample is transformed into the smectic A phase (see optical-microscopy snapshots in figure 3 and the video snapshot in supplementary data). With the above value of L and specific heat $c_p \sim 2 \text{ J gK}^{-1}$ [26], expecting the ECE of about 6–7 K in 14CB at a relatively low electric field sufficient to complete the I-SmA phase conversion is plausible.

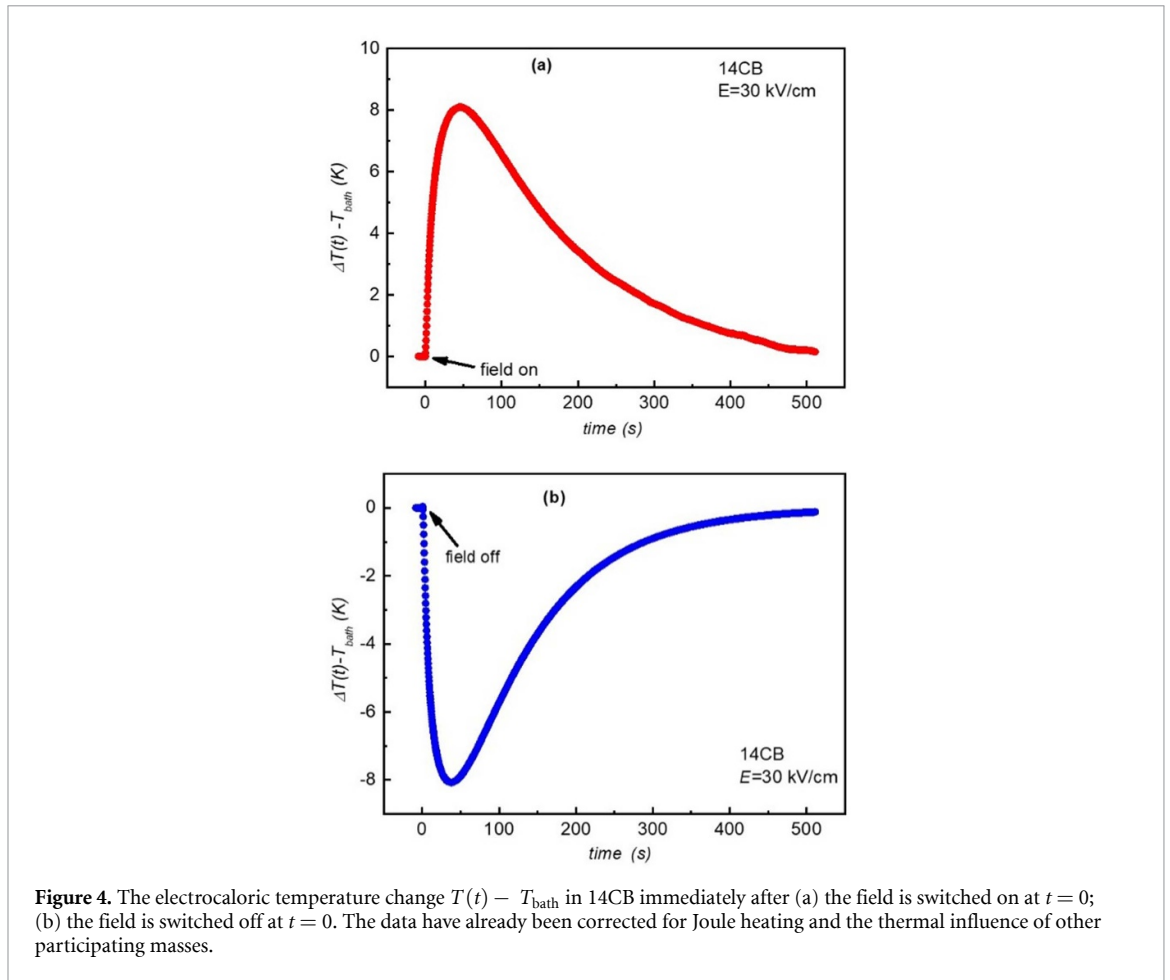


Figure 4. The electrocaloric temperature change $T(t) - T_{\text{bath}}$ in 14CB immediately after (a) the field is switched on at $t = 0$; (b) the field is switched off at $t = 0$. The data have already been corrected for Joule heating and the thermal influence of other participating masses.

2.2. Experimental results

Examples of the time evolution of the EC response, $T(t) - T_{\text{bath}}$, obtained in pure 14CB compound, in the vicinity of the I-SmA phase transition and after switching the electric field of 30 kV cm^{-1} on and off, are shown in figures 4(a) and (b), respectively. The EC response reaches a maximum value after a few tens of seconds, similar to what was observed in 12CB [23]. This slow response is because the fast EC response is convoluted by a longer internal thermal time of $\sim 20 \text{ s}$, in which the whole system reaches the internal thermal equilibrium. In addition, the data have already been corrected for Joule heating and the thermal influence of other participating masses.

Interestingly, a nearly symmetric EC response was observed upon field application and field removal due to the very small temperature hysteresis of the first-order I-SmA phase transition. The analysis of the relaxation tail $T(t)$ as described above, provides EC amplitude ΔT_{EC} , which value is typically 5% higher than the observed peaks.

Figure 4 shows the temperature dependence of the magnitude of the ECE temperature change ΔT_{EC} in the vicinity of the I-SmA transition in 14CB for the field application cycle (upper panel) and the field removal cycle (lower panel). The expected enhancement of the EC effect near the I-SmA phase transition temperature, denoted by T_c , is clearly seen in both panels of figure 5.

The maximum EC temperature change of 8.3 K was obtained in the cooling cycle for 14CB near the T_c , exceeding that of 12CB for about 2 K [23]. The I-SmA coexistence range is broadened from 180 mK in the absence of the electric field to about 2.5 K (see figure S4) by applying high electric fields, resulting in a more gradual decrease of the EC response as expected. However, the EC response still diminishes rapidly as the temperature is shifted away from the center of the I-SmA coexistence range. This is partially due to the increasingly reduced latent heat by approaching the edges of the coexistence range and partially due to the stiffening of the order parameter deeper in the smectic A phase, i.e., less changes of the order parameter can be induced by the electric field.

2.3. Discussion

In a way, obtaining the giant ECE in 14CB is not that surprising since an enhancement of the EC effect by the latent heat involved in the field-induced ferroelectric-paraelectric transition was demonstrated before

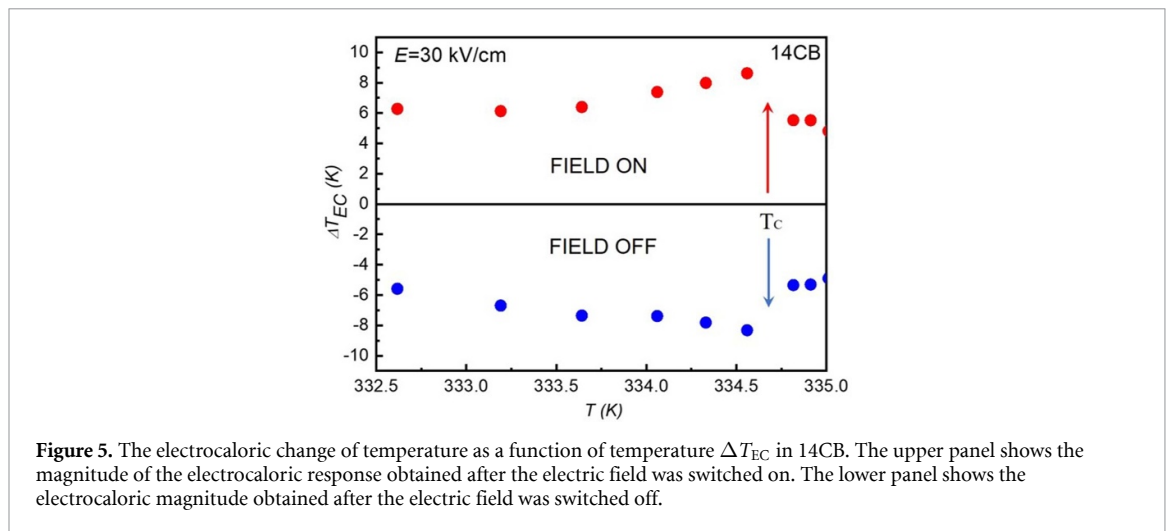


Figure 5. The electrocaloric change of temperature as a function of temperature ΔT_{EC} in 14CB. The upper panel shows the magnitude of the electrocaloric response obtained after the electric field was switched on. The lower panel shows the electrocaloric magnitude obtained after the electric field was switched off.

[2–11]. Nevertheless, the ECE enhancement in smectic LCs rivals the ECE response observed in the best solid-state ECs [11, 15, 36]. The largest EC effect was found in solids near the ferroelectric or antiferroelectric phase transitions [3] due to the relatively strong linear coupling between the polarization order parameter and the electric field and in PVDF-based polymers, due to their ability to sustain very high electric fields. In contrast, in LCs, there is only quadratic coupling between the order parameter S and the electric field E . However, the strong coupling between the orientational and the translational energy reservoirs results in an enhanced EC response with maximum EC responsivity $\Delta T_{EC}/E = 2.77 \times 10^{-6} \text{ Km V}^{-1}$ near the I-SmA transition temperature.

Most of the EC effect in 14CB can be attributed to the released/absorbed latent heat at the field-induced I-A or reversed A-I transition. Here, an estimation of the sample temperature change in the case that nearly all latent heat is involved in the EC effect gives $\Delta T_{EC} \sim L/c_p \sim 14.7 \text{ Jg}^{-1/2} \text{ Jg}^{-1} \text{ K}^{-1} \sim 7.3 \text{ K}$. The rest ($\sim 1 \text{ K}$) of the ECE stems from the continuous enthalpy contributions $\sim 2\text{--}3 \text{ Jg}^{-1}$ resulting from changes of the smectic and nematic order parameters induced by the electric field in agreement with previous observations in 5CB and 12CB [23, 24, 26]. The above results confirm that the critical fluctuations resulting in the continuous entropy changes near the isotropic to nematic or isotropic to smectic phase transition do not contribute substantially to the ECE in LC materials. In contrast, materials with substantial latent heat are the best candidates for soft materials with giant EC response. It was also shown recently that nanoparticle addition could significantly reduce the Joule heating in LCs [24]. It should be noted that due to large entropy changes, one could expect a significant barocaloric effect in LC materials.

3. eC effect in main-chain LCE: MC molecular simulations, experiment, and discussion

This section will present the eC effect in main-chain LCEs (MC-LCEs) by direct experimental methods and molecular simulations. There are two ways to enhance the eC response: (i) increasing the latent heat released at the first-order nematic-isotropic (N-I) phase transition or making the second-order N-I transition sharper. Similarly, as in the case of thermomechanical response [31], eCE improvements could be achieved by tuning the character of the nematic phase transition from a gradual supercritical towards a sharp first-order type by reducing the concentration of crosslinkers (χ) [31, 33]. Molecular MC simulation results will be presented first. Then the thermomechanical response and the direct measurements of the eC effect in main-chain LCEs will be discussed.

3.1. MC simulations

Our molecular MC simulations aim to provide an initial (mainly qualitative) insight into how the magnitude of the eC effect is affected by varying the concentration of crosslinkers in the sample. Here we follow the so-called indirect approach [15], wherein the reversible isothermal heat exchange is obtained by integrating the temperature derivative of strain (taken at constant stress) over stress. In this case, the simulation task boils down to getting the equation of the state of the system, i.e., the equilibrium relation between strain, stress, and temperature.

The simulation approach largely follows the steps presented in [37]. First, the mesogenic units embedded into our LCE samples are modeled by uniaxial ellipsoids with an aspect ratio of 3:1 interacting through the soft-core Gay-Berne (GB) potential [38, 39]. To prepare suitable monodomain samples, main-chain polymer

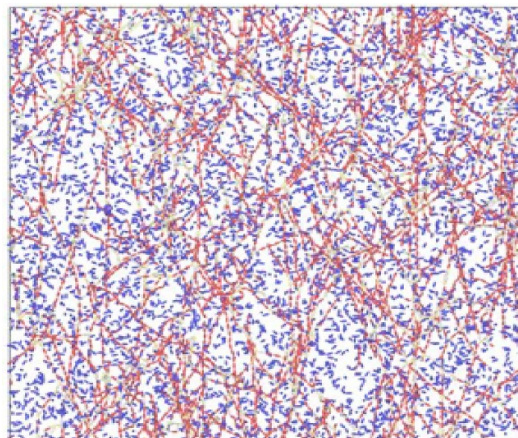


Figure 6. An example of a simulated sample in its reference state after a negative pressure shock to reveal the polymer network topology; only a thin slice is shown. The polymer strands (red ellipsoids) are aligned on average in the vertical direction, as imposed during sample preparation. The yellow and blue ellipsoids represent the crosslinks and the non-bonded swelling monomers, respectively.

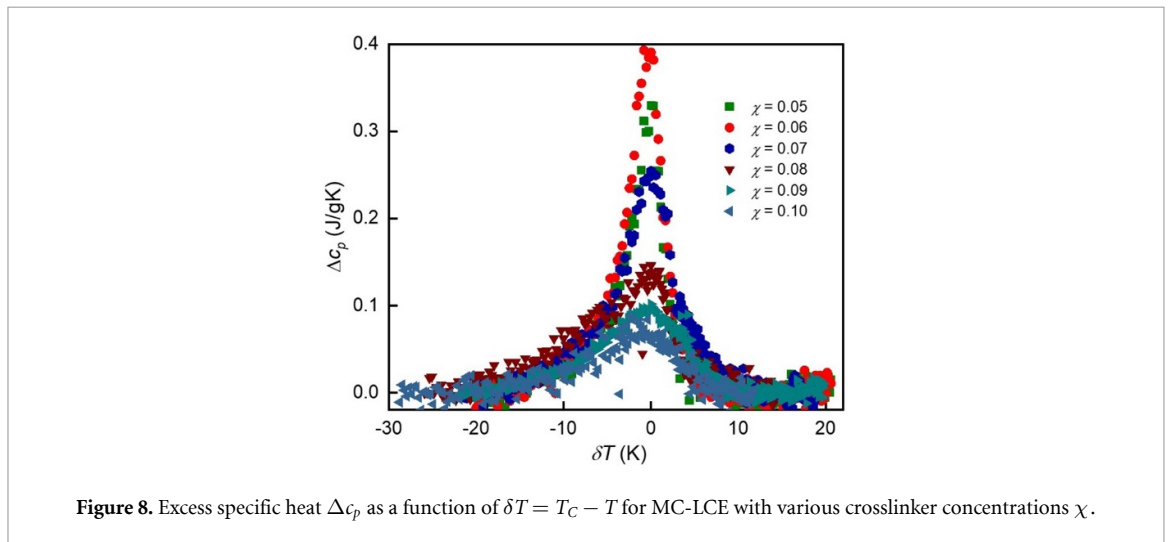
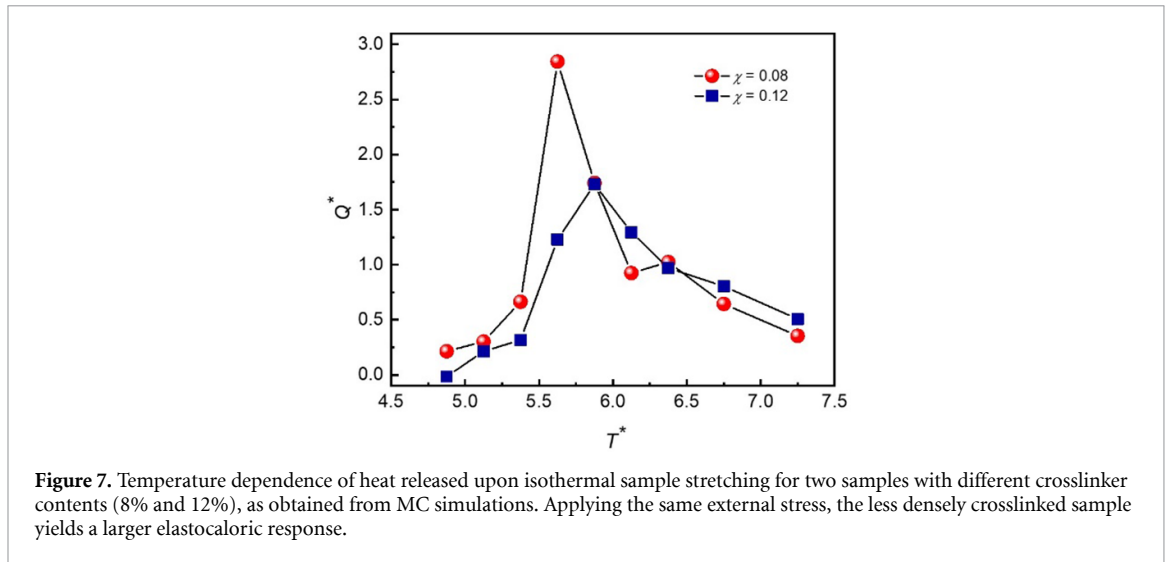
networks are created at low density in a cubic simulation box [40] under orientational bias [33] (like in the so-called Finkelmann two-step crosslinking procedure [32]). Next, the bonds between mesogens within the elastomer network are modelled via the finitely extensible nonlinear elastic potential [41], applied both to bond stretching and bending. Some ellipsoids are trifunctional and serve as crosslinkers; we consider two different samples with 8% and 12% crosslinker content. In addition, non-bonded swelling ellipsoids (50 vol. %) are introduced into the sample to enhance MC equilibration while still conveying nematicity before finally isotropically compressing the sample nearly to close-packing. As a result, a cubic ‘reference’ sample is obtained, containing a total of $N = 64\,000$ GB particles. Periodic boundary conditions are assumed at simulation box boundaries to mimic a larger bulk sample. Figure 6 shows a slice of a typical ‘reference’ sample after a negative pressure shock, revealing the structure of the polymer network. Then, the equilibrium sample configurations were obtained by performing constant-stress MC simulations, employing a modified Metropolis algorithm wherein both temperature (T) and external engineering stress (σ) are fixed [42]. For more details, consult [37] and the references therein.

The eC response of LCE samples with two different crosslinking densities, as obtained from simulations, is shown in figure 7. The heat released upon isothermal external stress application peaks near the nematic-isotropic phase transition and is larger in the less densely crosslinked sample. Figure 7 shows the reduced heat $Q^* = Q/\varepsilon_0 N$ (per particle and in units of ε_0 , the characteristic interaction energy scale of the GB potential) versus reduced temperature $T^* = k_B T/\varepsilon_0$ when a reduced engineering stress $\sigma^* = 0.06$ is applied. (Here, the stress $\sigma = \sigma^* \varepsilon_0/\sigma_0^3$, where σ_0 is the short axis of a GB ellipsoid.) Taking $\varepsilon_0 = 9.3 \times 10^{-22}$ J and $\sigma_0 = 10^{-9}$ m [40], this places the N-I transition at around 380 K, and the heat Q released by the better-performing $\chi = 8\%$ sample equals approximately 1.7 kJ mol $^{-1}$ when an external stress of 56 kPa is applied. Assuming further that the GB ellipsoids represent LCE mesogens whose kilomolar mass equals 537 kg kmol $^{-1}$ and taking 2 kJ kgK $^{-1}$ as a specific heat estimate, this translates into an eC temperature change $\Delta T_{eC} \approx 1.6$ K if the experiment was performed under adiabatic conditions, as it is usual in measurements following the direct approach. From here we can predict a relatively high eC responsivity $\Delta T_{eC}/\Delta\sigma = 28$ K MPa $^{-1}$ at a low-stress field of $\Delta\sigma = 0.056$ MPa.

The MC simulations demonstrate that (i) a relatively small stress field could induce a rather sizable eCE with good eCE responsivity, and (ii) the eCE response increases with decreasing the concentration of the crosslinkers, which drives, as shown in experiments, the LCE system toward the critical point [31, 33].

3.2. Experimental

The MC-LCE sample preparation followed the conventional two-step Finkelmann procedure described in [32]. The 1,1,3,3-Tetramethyldisiloxane is used as a polymer chain extender, and the 2,4,6,8,10-Pentamethylcyclopentasiloxane as a five-point crosslinker. The chemical structure of an LC mesogen is shown in figure S5 [33]. Toluene was used as a solvent, and a solution of dichloro(1,5-cyclooctadiene) platinum(II) in dichloromethane as a catalyst. The second crosslinking step was carried out in the nematic phase. Several MC-LCEs of different crosslinker concentrations, $\chi = 0.05, 0.06, 0.07, 0.08, 0.09$, and 0.10 , were synthesized to sharpen the nematic phase transition by tuning its nature across the critical point from the supercritical to the first-order type.



A homemade setup was used for eC and thermomechanical measurements (figure S6), which can measure length, strain, and temperature simultaneously. LCE samples in the form of strips are cut to a length l , typically ranging from a few mm to several cm. A small bead thermistor was glued to the sample's surface, which was then connected to glass holders and inserted into our homemade setup. An image of a prepared sample is given in figure S7. The sample is inserted into a copper block with an attached heater. The temperature of the copper block is stabilized with a Lakeshore model 350 temperature controller. The precision gram sensor, capable of measuring compression and tension, is used to measure stress (figure S8) experienced by the LCE samples.

As described in [2], the relaxation of the temperature of the whole LCE sample system to the bath temperature was analyzed, similarly to the ECE data in LCs. The eC temperature change of the LCE sample system was determined by considering the heat capacities of its constituents, C_p^i , such as the LCE sample, glues, thermistor, and attaching wires, $\Delta T_{eC} = \Delta T \sum_i C_p^i / C_p^{eC}$. Again, C_p^{eC} stands for the heat capacity of the eC active LCE material, i.e., part of LCE not rigidly glued to the supporting rods. More details on sample preparation and data analysis can be found in the supplemental data (figure S9).

3.3. Experimental results

In order to determine the nature of the nematic phase transition in MC-LCE samples with different crosslinking concentrations χ , the temperature evolution of the specific heat capacity c_p was measured by a high-resolution calorimeter [43]. Figure 8 shows the excess specific heat Δc_p as a function of $\delta T = T_C - T$, where T_C represents the nematic phase transition temperature. Here, the noncritical thermal background was subtracted from the specific heat c_p .

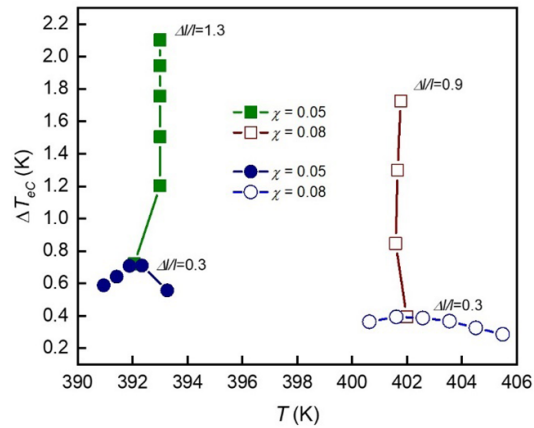


Figure 9. The elastocaloric response ΔT_{eC} as a function of temperature T . Solid and open circles show the $\Delta T_{eC}(T)$ at $\Delta l/l = 0.3$. The solid and open boxes represent $\Delta T_{eC}(\Delta l/l)$ measured at the constant peak-position temperature.

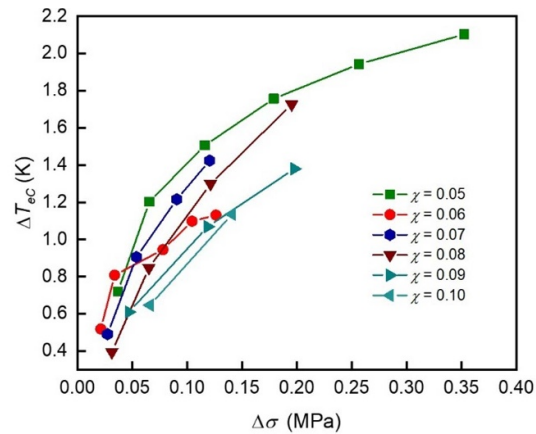


Figure 10. The eC temperature change ΔT_{eC} in MC-LCEs with different compositions χ as a function of stress-field change $\Delta\sigma$.

The excess specific heat data of MC-LCEs with crosslinker concentrations $\chi = 0.05, 0.06, 0.07, 0.08, 0.09,$ and 0.10 show that with increasing crosslinker concentration, the phase transition changes from being weakly first-order at lowest crosslinker concentration ($\chi = 0.05$) to second-order critical at 0.06 and supercritical at higher crosslinker concentrations ($\chi \geq 0.07$). The relaxation calorimetry confirmed that only the $\chi = 0.05$ sample had a small detectable amount of latent heat, $L = 0.096 \text{ J gK}^{-1}$. In contrast to our previous results [33], the current synthesized MC-LCE system enables studies of the eCE in the vicinity and below the critical point.

Measurements of the thermomechanical response additionally confirm calorimetric results, i.e., samples with lower crosslinker concentration exhibit sharper phase transition. Figure S9 shows the relative extension of the samples λ , as a consequence of the thermomechanical response for three samples with crosslinker concentrations $\chi = 0.06, 0.07,$ and 0.08 . It is evident that with lower χ the transition becomes sharper and thus, larger eC temperature change ΔT_{eC} is expected at lower χ .

Typical examples of direct eCE measurements at different temperatures of MC-LCEs with $\chi = 0.05$ and $\chi = 0.08$ are shown in figure 9. Each sample was stretched for a specific relative extension $\Delta l/l$ near the phase transition temperature. Measurements of ΔT_{eC} temperature variation, performed at lower stress fields, i.e., smaller $\Delta l/l$, allowed the determination of the temperature position of the expected maximums in ΔT_{eC} . At these temperatures of expected maximum response, ΔT_{eC} was then measured for higher values of $\Delta l/l$ (see figure 9). These *peak position* values of ΔT_{eC} were later used in figures 10 and 11.

Figure 10 shows the eC *peak position* values of ΔT_{eC} as a function of applied stress $\Delta\sigma$ measured at the temperature of the maximum response as described above. As expected, the largest $\Delta T_{eC} = 2.1 \text{ K}$ was obtained in the $\chi = 0.05$ sample. The critical composition $\chi = 0.06$ shows a peculiar crossover from the largest ΔT_{eC} at low applied stress to lower ΔT_{eC} at higher $\Delta\sigma$. This could be a consequence of the shift of sample state away from the critical point (at which only the transition is continuous) by higher values of $\Delta\sigma$ in a 3D phase diagram ($\chi, T, \Delta\sigma$), similar to what was found in relaxor ceramics PMN-PT [36, 43]. For

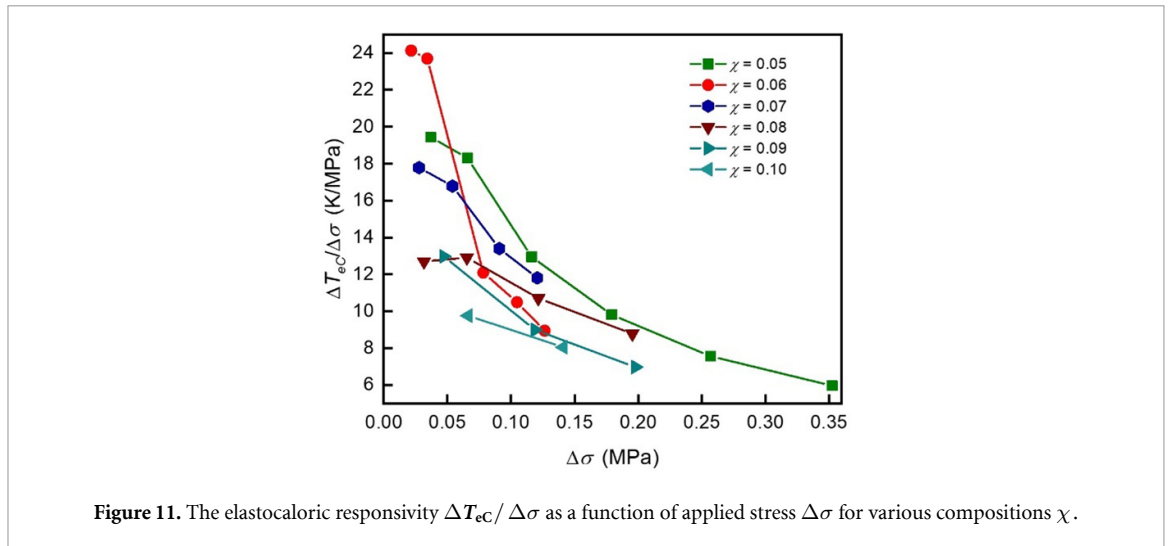


Figure 11. The elastocaloric responsivity $\Delta T_{eC}/\Delta\sigma$ as a function of applied stress $\Delta\sigma$ for various compositions χ .

compositions $\chi > 0.06$, the eC response systematically drops with increasing composition as the nematic transition becomes more and more supercritical, i.e., smeared.

Figure 11 shows the eC responsivity $\Delta T_{eC}/\Delta\sigma$ as a function of the applied stress $\Delta\sigma$, again measured at the temperature of the maximum response. Similar to the relaxor ferroelectrics [36], at low applied stress $\Delta\sigma$, the critical composition $X = 0.06$ has the highest eC responsivity $\Delta T_{eC}/\Delta\sigma = 24.2 \text{ K MPa}^{-1}$, which for higher applied stress $\Delta\sigma$ values rapidly drop. The other compositions follow a similar pattern, with the $X = 0.05$ sample displaying the largest $\Delta T_{eC}/\Delta\sigma$ at lower stress values.

Such behavior of eC responsivity similar to that found in the disordered relaxor ferroelectrics [36] is not surprising, as MC-LCEs can be treated as nematic materials with the quenched disorder [44].

3.4. Discussion

The above results of eC response in MC-LCEs with varying crosslinker concentrations demonstrate that materials near the critical point or below, i.e., first-order samples, exhibit larger eC responsivity and ΔT_{eC} at relatively moderate stress fields, in good qualitative agreement with MC simulations. The experiments also show that samples with lower crosslinker concentrations are less prone to tearing at larger applied stresses.

4. Conclusion

In conclusion, we have presented an overview of investigations of the EC and eC effects in soft LCs and LCEs, respectively. Specifically, by direct EC experiments, it was demonstrated that strong coupling between the nematic orientational and smectic translational energy reservoirs leads to an enhanced EC response in smectic 14CB LC with large EC temperature change ΔT_{eC} of 8.3 K and giant EC responsivity $\Delta T_{eC}/E = 2.77 \times 10^{-6} \text{ Km V}^{-1}$ near the isotropic to smectic A transition temperature. Despite the weaker quadratic coupling with the nematic order parameter through the dielectric tensor anisotropy, both values rival the best values obtained in solid materials. The EC responsivity is an order of magnitude higher than the average EC responsivity in relaxor ferroelectrics. The phase-changing LC materials with large latent heat are thus an excellent candidate for thermal stabilization and thermal transport applications [45]. As fluids, they can also play a role of an EC active regeneration material which can reduce the passive mass in cooling devices employing the regeneration technique [11, 19].

Furthermore, by MC simulations and direct eC experiments, the eC effect in main-chain LCE of different crosslinking compositions was investigated. Numerical MC and phenomenological simulations predicted the highest eC response in main-chain LCE materials with the lower density of crosslinkers, i.e., with the imprinted stress field low enough to drive the system near or below the liquid-vapor type critical point. MC-LCEs with different crosslinker concentrations ranging from $= 0.05$ – 0.10 were synthesized. High-resolution specific heat data and measurements of the thermomechanical response confirm that the nematic phase transition sharpens by tuning its nature across the critical point (at $= 0.06$) from the supercritical (≥ 0.07) to the first-order type ($= 0.05$). Direct eC experiments confirm the enhancement of the eC response by the latent heat and sharpness of the nematic phase transition. The largest $\Delta T_{eC} = 2.1 \text{ K}$ was obtained in the $= 0.05$ sample at $\Delta\sigma = 0.35 \text{ MPa}$. It should be noted that the highest eC responsivity $\Delta T_{eC}/\Delta\sigma = 24.2 \text{ K MPa}^{-1}$ was obtained at a low-stress field of $\Delta\sigma = 0.02 \text{ MPa}$ in good qualitative agreement with MC simulation results. Such MC-LCE's eC responsivity is three orders of magnitude larger

than the average eC responsivity found in the best shape memory alloys. Interestingly, the general stress dependence of the eC responsivity of MC-LCE nematic-quenched-disordered materials is similar to that found in disordered relaxor ferroelectrics [36, 44]. The MC-LCEs could be used in eC devices of similar construction as described in [7]. Here, the passive regeneration fluid could be replaced by caloric active LCs potentially exhibiting a significant mC effect.

The observed large caloric responses in soft LC-based materials that can be induced by much smaller fields in contrast to solid caloric materials, and the ability to control their thermal and electrical conductivity by the addition of nanoparticles, demonstrate their potential application as new cooling elements, caloric-active regeneration materials, and elements of thermal diodes in new heat-management devices.

Data availability statement

All data that support the findings of this study are included within the article (and any supplementary files).

Acknowledgments

This work was partially supported by the European Commission Grant 778072 H2020-MSCA-RISE-2017, European Regional Development Fund, and Slovenian Research and Innovation Agency grants [J1-9147, L1-2607, P1-0099, and P1-0125].












Credit authorship contribution statement

Dejvid Črešnar: eCE in LCEs investigation, Formal analysis, Validation, Visualization; Marta Lavrič: eCE in LCEs investigation, Formal analysis, Validation, Visualization; Maja Trček: ECE in LCs investigation, Formal analysis; Zdravko Kutnjak: Resources, Funding acquisition, Conceptualization, Methodology, Supervision, Writing—Review & Editing; Brigita Rožič: Investigation, Supervision, Writing—Original Draft & Review & Editing, Visualization; Nikita Derets, Andraž Rešetič, Boštjan Zalar, Valentina Domenici: LCEs synthesis and characterization, Funding acquisition, Supervision; Gregor Skačej: LCEs Monte Carlo modeling, Investigation, Writing—Editing; Samo Kralj: ECE and eCE modelling, Supervision.

Conflict of interest

The authors declare that they have no known competing financial interests or personal relationships that could have appeared to influence the work reported in this paper.

ORCID iDs

Dejvid Črešnar  <https://orcid.org/0000-0002-6684-4500>
Nikita Derets  <https://orcid.org/0000-0001-5271-1638>
Maja Trček  <https://orcid.org/0000-0001-6012-752X>
Gregor Skačej  <https://orcid.org/0000-0002-8849-6877>
Andraž Rešetič  <https://orcid.org/0000-0003-2851-4401>
Marta Lavrič  <https://orcid.org/0000-0003-3287-8910>
Valentina Domenici  <https://orcid.org/0000-0003-3155-8384>
Boštjan Zalar  <https://orcid.org/0000-0002-1260-6697>
Samo Kralj  <https://orcid.org/0000-0002-3962-8845>
Zdravko Kutnjak  <https://orcid.org/0000-0002-3089-7993>
Brigita Rožič  <https://orcid.org/0000-0002-4577-7847>

References

- [1] McLinden M O, Brown J S, Brignoli R, Kazakov A F and Domanski P A 2017 Limited options for low-global-warming-potential refrigerants *Nat. Commun.* **8** 14476
- [2] Correia T and Zhang Q (eds) 2014 *Electrocaloric Materials* (Springer) (<https://doi.org/10.1007/978-3-642-40264-7>)
- [3] Kutnjak Z, Rožič B and Pirc R 2015 Electrocaloric effect: theory, measurements, applications *Wiley Encyclopedia of Electrical and Electronics Engineering* (Wiley) pp 1–19
- [4] Valant M 2012 Electrocaloric materials for future solid-state refrigeration technologies *Prog. Mater. Sci.* **57** 980–1009
- [5] Moya X and Mathur N D 2020 Caloric materials for cooling and heating *Science* **370** 797–803
- [6] Liu J, Zhao D and Li Y 2017 Exploring magnetic elastocaloric materials for solid-state cooling *Shape Mem. Superelasticity* **3** 192–8
- [7] Tušek J, Engelbrecht K, Eriksen D, Dall'Olio S, Tušek J and Pryds N 2016 A regenerative elastocaloric heat pump *Nat. Energy* **1** 16134

- [8] Chen X, Zhu W, Rattner A S and Zhang Q M 2023 A self-actuated electrocaloric polymer heat pump design exploiting the synergy of electrocaloric effect and electrostriction *J. Phys. Energy* **5** 024009
- [9] Mischenko A S, Zhang Q, Scott J F, Whatmore R W and Mathur N D 2006 Giant electrocaloric effect in thin-film $\text{PbZr}_{0.95}\text{Ti}_{0.05}\text{O}_3$ *Science* **311** 1270–1
- [10] Pirc R, Kutnjak Z, Blinc R and Zhang Q M 2011 Electrocaloric effect in relaxor ferroelectrics *J. Appl. Phys.* **110** 074113-1-074113-7
- [11] Moya X, Defay E, Heine V and Mathur N D 2015 Too cool to work *Nat. Phys.* **11** 202–5
- [12] Rožič B, Malič B, Uršič H, Holc J, Kosec M, Neese B, Zhang Q M and Kutnjak Z 2010 Direct measurements of the giant electrocaloric effect in soft and solid ferroelectric materials *Ferroelectrics* **405** 26–31
- [13] Tishin M and Spichkin Y I 2003 *The Magnetoelectric Effect and Its Applications* (Institute of Physics Publishing) (<https://doi.org/10.1201/9781420033373>)
- [14] Lu S G et al 2010 Organic and inorganic relaxor ferroelectrics with giant electrocaloric effect *Appl. Phys. Lett.* **97** 162904-1–3
- [15] Moya X, Kar-Narayan S and Mathur N D 2014 Caloric materials near ferroic phase transitions *Nat. Mater.* **13** 439–50 and references therein
- [16] Neese B, Chu B, Lu S-G, Wang Y, Furman E and Zhang Q M 2008 Large electrocaloric effect in ferroelectric polymers near room temperature *Science* **321** 821–3
- [17] Lu S G, Rožič B, Zhang Q M, Kutnjak Z, Pirc R, Lin M, Li X and Gorny L J 2010 Comparison of directly and indirectly measured electrocaloric effect in relaxor ferroelectric polymers *Appl. Phys. Lett.* **97** 202901-1-202901-3
- [18] Gu H, Qian X, Li X, Craven B, Zhu W, Cheng A, Yao S C and Zhang Q M 2013 A chip scale electrocaloric effect based cooling device *Appl. Phys. Lett.* **102** 122904-1–3
- [19] Plaznik U, Kitanoški A, Rožič B, Malič B, Uršič H, Drnovšek S, Cilenšek J, Vrabelj M, Poredoš A and Kutnjak Z 2015 Bulk relaxor ferroelectric ceramics as a working body for an electrocaloric cooling device *Appl. Phys. Lett.* **106** 043903-1–4
- [20] Lelidis I and Durand G 1996 Electrothermal effect in nematic liquid crystal *Phys. Rev. Lett.* **76** 1868–71
- [21] Lelidis I, Nobili M and Durand G 1993 Electric-field-induced change of the order parameter in a nematic liquid crystal *Phys. Rev. E* **48** 3818–21
- [22] Qian X-S, Lu S-G, Li X, Gu H, Chien L-C and Zhang Q M 2013 Large electrocaloric effect in a dielectric liquid possessing a large dielectric anisotropy near the isotropic-nematic transition *Adv. Funct. Mater.* **23** 2894–8
- [23] Trček M, Lavrič M, Cordoyiannis G, Zalar B, Rožič B, Kralj S, Tzitiou V, Nounesis G and Kutnjak Z 2016 Electrocaloric and elastocaloric effects in soft materials *Phil. Trans. Math. Phys. Eng. Sci.* **374** 20150301-1–11
- [24] Klemenčič E, Trček M, Kutnjak Z and Kralj S 2019 Giant electrocaloric response in smectic liquid crystals with direct smectic-isotropic transition *Sci. Rep.* **9** 1721-1–10
- [25] Mañosa L, Stern-Taulats E, Gràcia-Condal A and Planes A 2023 Cross-coupling contribution to the isothermal entropy change in multicaloric materials *J. Phys. Energy* **5** 024016
- [26] Thoen J 2009 Investigations of phase transitions in liquid crystals by means of adiabatic scanning calorimetry *Liq. Cryst.* **36** 669–84
- [27] Li J, Torelló A, Nouchokgwe Y, Granzow T, Kovacova V, Hirose S and Defay E 2023 Electrocaloric effect in BaTiO_3 multilayer capacitors with first-order phase transitions *J. Phys. Energy* **5** 024017
- [28] Pieczyska E A, Gadaj S P, Nowacki W K and Tobushi H 2006 Phase-transformation fronts evolution for stress- and strain-controlled tension tests in TiNi shape memory alloy *Exp. Mech.* **46** 531–42
- [29] Kabirifar P, Trojer J, Brojan M and Tušek J 2022 From the elastocaloric effect towards an efficient thermodynamic cycle *J. Phys. Energy* **4** 044009
- [30] Qian S, Catalini D, Muehlbauer J, Liu B, Mevada H, Hou H, Hwang Y, Radermacher R and Takeuchi I 2023 High-performance multimode elastocaloric cooling system *Science* **380** 722–7
- [31] Wim H D J 2012 *Liquid Crystal Elastomers: Materials and Applications* (Springer) (<https://doi.org/10.1007/978-3-642-31582-4>)
- [32] Küpfer I and Finkelmann H 1991 Nematic liquid single crystal elastomers *Makromol. Chem. Rapid Commun.* **12** 717–26
- [33] Lavrič M et al 2021 Tunability of the elastocaloric response in main-chain liquid crystalline elastomers *Liq. Cryst.* **48** 405–11
- [34] Aravindhan A, Lheritier P, Torelló A, Prah U, Nouchokgwe Y, El Moul A, Chevalier X, Dos Santos F D, Defay E and Kovacova V 2023 Direct measurement of electrocaloric effect in P(VDF-TrFE-CFE) film using infrared imaging *J. Mater.* **9** 256–60
- [35] Kholkin A L, Pakhomov O V, Semenov A A and Tselev A 2023 *The electrocaloric effect: materials and applications* (Woodhead Publishing Series in Electronic and Optical Materials) (available at: <https://books.google.si/books?id=uYGEEAAAQBAJ>)
- [36] Rožič B, Kosec M, Uršič H, Holc J, Malič B, Zhang Q M, Blinc R, Pirc R and Kutnjak Z 2011 Influence of the critical point on the electrocaloric response of relaxor ferroelectrics *J. Appl. Phys.* **110** 064118
- [37] Skačej G 2018 Elastocaloric effect in liquid crystal elastomers from molecular simulations *Liq. Cryst.* **45** 1964
- [38] Berardi R, Zannoni C, Lintuvuori J S and Wilson M R 2009 A soft-core Gay-Berne model for the simulation of liquid crystals by Hamiltonian replica exchange *J. Chem. Phys.* **131** 174107
- [39] Gay J G and Berne B J 1981 Modification of the overlap potential to mimic a linear site-site potential *J. Chem. Phys.* **74** 3316–9
- [40] Skačej G and Zannoni C 2014 Molecular simulations shed light on supersoft elasticity in polydomain liquid crystal elastomers *Macromolecules* **47** 8824
- [41] Bird R B, Armstrong R C and Hassager D 1977 *Dynamics of Polymeric Liquids* (Wiley)
- [42] Frenkel D and Smit B 2002 *Understanding Molecular Simulation: From Algorithms to Applications* (Academic)
- [43] Kutnjak Z, Petzelt J and Blinc R 2006 The giant electromechanical response in ferroelectric relaxors as a critical phenomenon *Nature* **441** 956–9
- [44] Petridis L and Terentjev E M 2006 Nematic-isotropic transition with quenched disorder *Phys. Rev. E* **74** 051707
- [45] Krašna M, Klemenčič E, Kutnjak Z and Kralj S 2018 Phase-changing materials for thermal stabilization and thermal transport *Energy* **162** 554–63